Supporting Information

Adjustable and Low-Cost Production of Magnesium Alloys Using a Liquid Metal Cathode

Zefa Qin,[1,2] Junchen Li,[1,2] Yang Song,[1] Jiangfeng Song, [1] Liwen Hu, [1,2,*] Xuewei Lv, [1,2,*] Xianhua Chen,[1] Fusheng Pan[1]

[1]*College of Materials Science and Engineering, Chongqing University, Chongqing 400044, PR China*

[2]*Chongqing Key Laboratory of Vanadium-Titanium Metallurgy and New Materials, Chongqing University, Chongqing 400044, PR China*

***Corresponding author:** Liwen Hu, Xuewei Lv

E-mail: lwh0423@cqu.edu.cn, lvxuewei@cqu.edu.cn

Address: College of Materials Science and Engineering, Chongqing University, Chongqing 400044, PR China

1.1. Materials and Reagents

The electrolytes were comprised of NaCl (AR), KCl (AR), $MgCl_2$ (AR), $CaCl_2$ (AR), KF (AR), and Sn (99.99%), Zn (99.99%), Al (99.99%) particles were purchased from Shanghai Aladdin Biochemical Technology Co., Ltd. Mo, W, and Stainless steel rods used as conductive rods were purchased from Jiaming Platinum Industry Co. Ltd.

The electrolyte was pre-dried in an alumina crucible under vacuum by heating it from ambient temperature to 573 K and then maintaining it for 12 h. Afterward, the cooled and pre-dried electrolyte was placed in a glove box. All experiments were conducted in a sealed vessel under a dried argon atmosphere at 973 K.

1.2. Computational details and methods

The Gibbs free energy for Mg alloy deposition was calculated using HSC software, and the reaction potential was determined using the Nernst equation, as presented in **Table S2**. COMSOL Multiphysics 6.1 was used to simulate the diffusion of Mg in Sn, and the model was established with the Mg influx rate at the interface being 233t $mol \cdot m^{-3} \cdot min^{-1}$ and the Mg diffusion coefficient being 10^{-8} $m^2 \cdot s^{-1}$ [1]. The liquid metal model was established by Amorphous Cell, and then the Geometry Optimization - Anneal - Dynamics under the Compass II forcefield were performed using the Forcite module. The kinetic characterization is performed in 5000 steps within 5ps using the canonical ensemble (NVT) system synthesis. The Andersen pressure control method and Nose temperature control method were adopted. Atoms are added into the cell according to

the molar ratio, and the cell parameters are adjusted to ensure that the density is consistent with the theory. The binding energy calculation is based on the simulation results of Mg^{2+} and base metal.

All DFT calculations were performed using the Vienna ab initio simulation package (VASP) with a generalized gradient approximation (GGA) based on exchange-correlation function parameterizations including Perdew, Burke, and Ernzerhof (PBE) [2]. Our study utilized the Gamma-centered Monkhorst-Pack grid with (3 × 3 × 1) k-point sampling across all systems, complemented by a cut-off plane wave basis set to 500 eV. Electronic structure iterations adhered to standard settings of 1×10^{-5} eV and 0.001 eV $Å^{-1}$.

Mg^{2+}, which exists in molten electrolytes, will be adsorbed on the surface of a liquid metal cathode substrate under the action of the electric field. The adsorption process of ions to the substrate satisfies the following **Eq. (1)** [3]:

$$\Delta\mu_{S/M} = k\Delta G_{BE} + \Delta\mu_0 = ze_0(U_p - U_0) = ze_0\Delta U_p \quad (1)$$

Thus,

$$\Delta U_p = \frac{k}{ze_0}\Delta G_{BE} + \frac{\Delta\mu_0}{ze_0} \quad (2)$$

Where ΔG_{BE} is the binding energy, $\Delta\mu_{S/M}$ is the potential difference between the substrate and the metal, μ is the chemical potential in atomic units, e_0 is the electronic charge, U_0 and U_p represent the energy of the substrate before and after adsorption, z is the number of substances, k is the coefficient, respectively. Hence, the adsorption ability of Mg^{2+} on the metal substrate can be determined by the binding energy.

1.3. Electrochemical measurements

The entire experiment was conducted under an argon atmosphere using a three-electrode system. The blank melt was 207.5 g NaCl-KCl-$CaCl_2$ = 48:34:18 (wt.%). The working electrodes consisted of an inert tungsten (W) wire (0.3 mm in diameter, 99.99% purity) and liquid tin (Sn) (3 mm in diameter, 99.99% purity). A graphite rod (10 mm in diameter, 99.99% purity) was used as the counter electrode, while a quasi-reference electrode was made of silver (Ag) wire (0.5 mm in diameter, 99.99% purity). The W wire working electrode was immersed into the molten salt to a depth of 3.0 mm. Electrochemical measurements, including cyclic voltammetry, square wave voltammetry, chronopotentiometry, and open circuit potential, were performed using a VersaSTAT 3F to investigate the electrochemical behavior of Mg^{2+}.

1.4. Electrolysis of $MgCl_2$ using liquid Sn cathode

We improved the current efficiency by changing parameters such as electrolyte concentration, current density, and anode working area, and selected the optimal parameters as the electrolysis parameters of the liquid metal cathode (**Table S3**). 5 g KF was added to the molten salt to weaken the effect of MgO. The mass fraction of $MgCl_2$ was increased to 15%. Pre-electrolysis was conducted at 973 K to eliminate residual impurities in the molten salt. A constant voltage of 1.5 V was applied between the C anode and the Mo cathode for 3 hours. Subsequently, the Sn cathode was prepared by placing 1 g Sn metal in an Al_2O_3 crucible fitted with a stainless steel rod encased in an Al_2O_3 tube. The Al_2O_3 crucible was positioned at the bottom of the electrolysis setup,

as depicted in **Fig. S2**. Electrolysis was performed at 973 K under a constant current of 0.4 $A \cdot cm^{-2}$ for 5.5/8.8/14.7 hours. After electrolysis, samples were collected from the surface of the electrolytic cell and the bottom of the Al_2O_3 crucible, and then polished.

Supplementary Figures

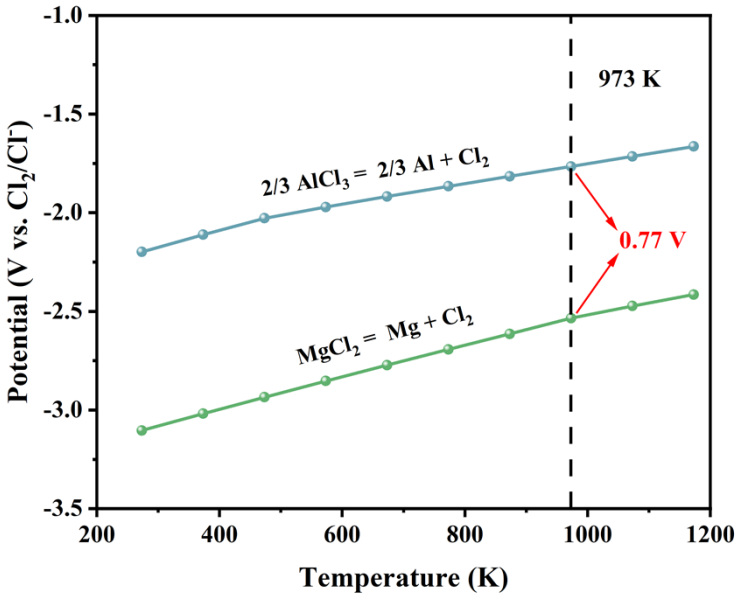

Fig. S1. Theoretical decomposition potentials of $MgCl_2$ and $AlCl_3$.

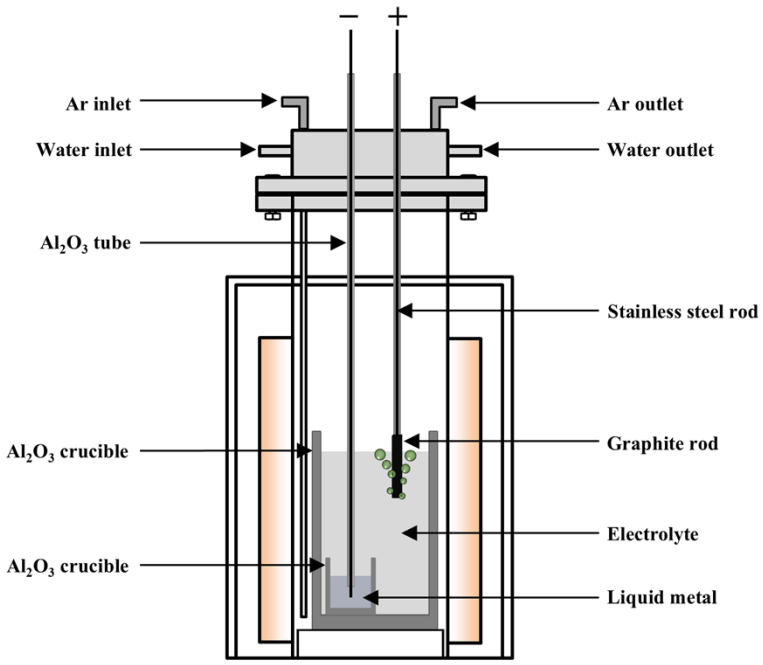

Fig. S2. Schematic diagram of electrodeposition device.

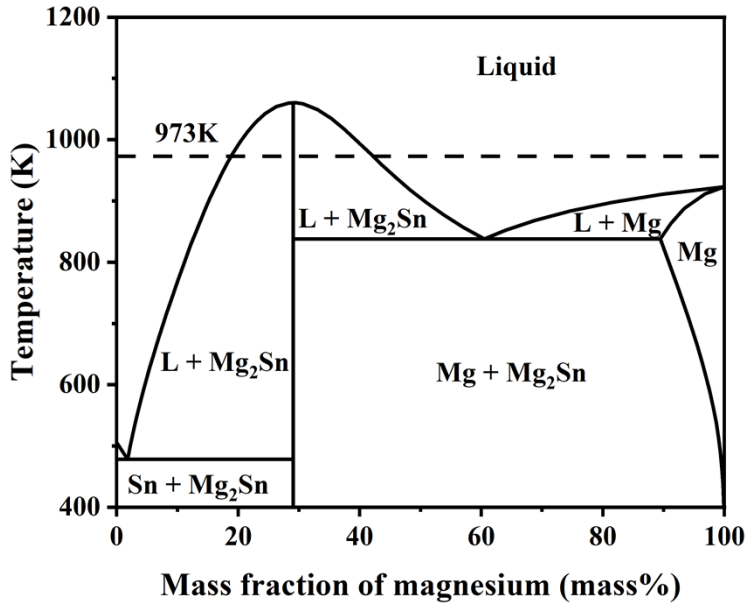

Fig. S3. Binary phase diagram of Mg and Sn.

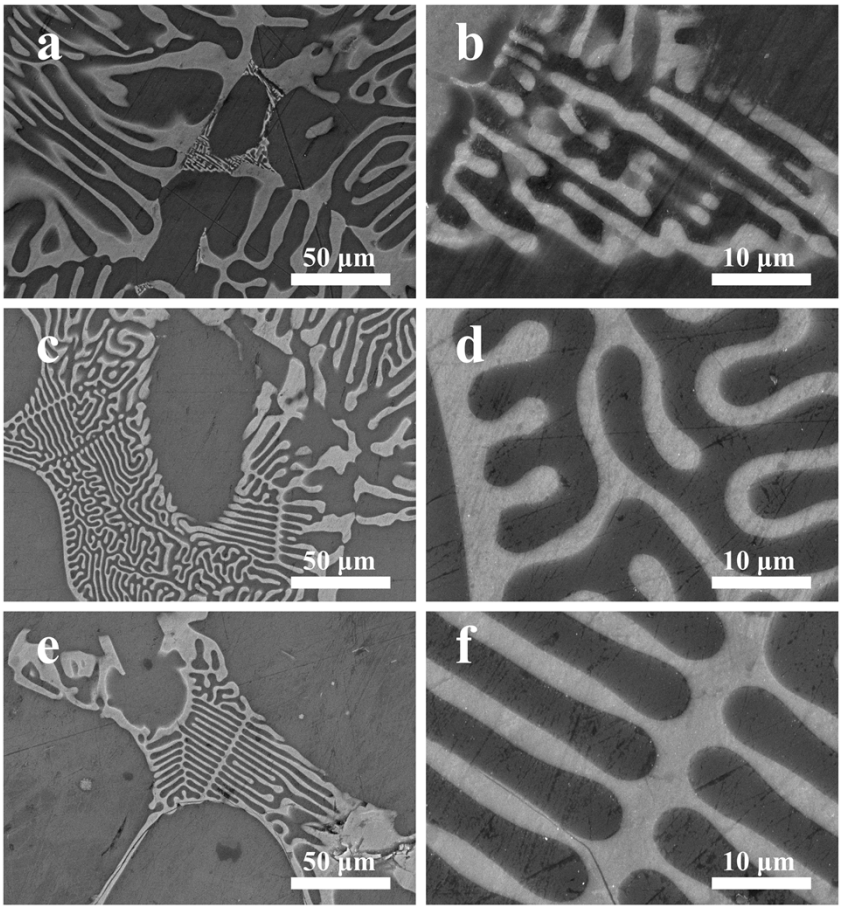

Fig. S4. SEM images of (a-b) Mg60Sn40, (c-d) Mg70Sn30, and (e-f) Mg80Sn20.

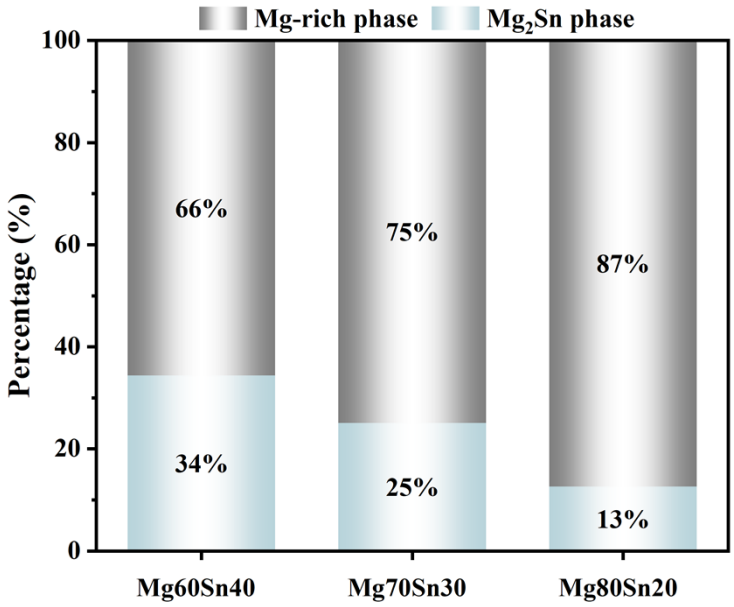

Fig. S5. The proportion of the Mg-rich and Mg_2Sn phase of **Figs. 2d-f**.

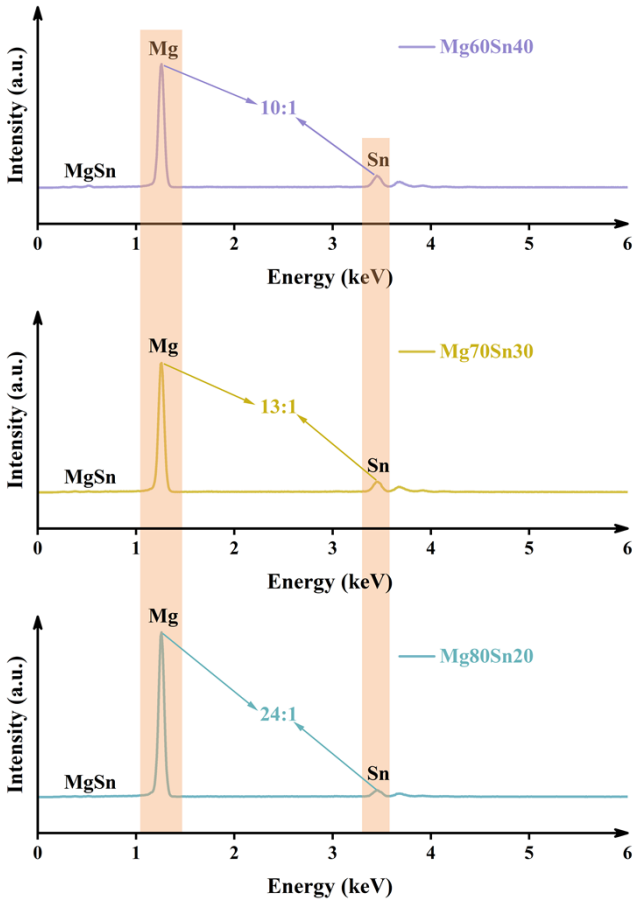

Fig. S6. The element content of corresponding EDS mapping images.

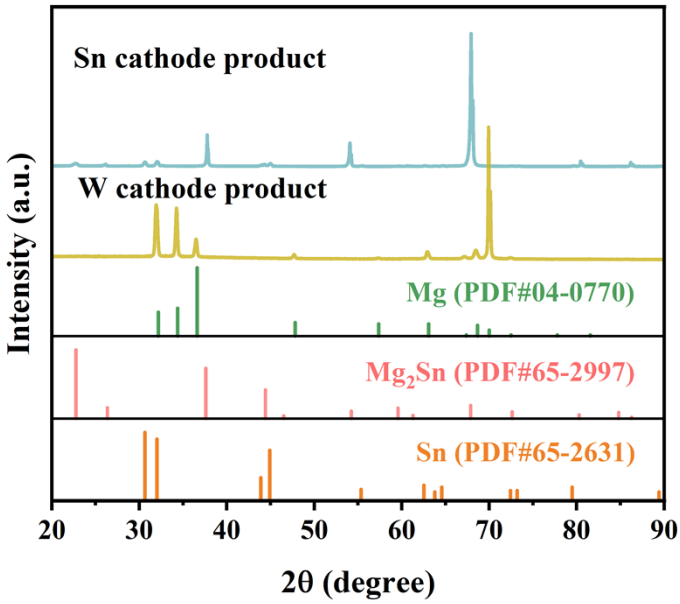

Fig. S7. XRD patterns of the electrolysis products on W and Sn cathodes under identical Mg production.

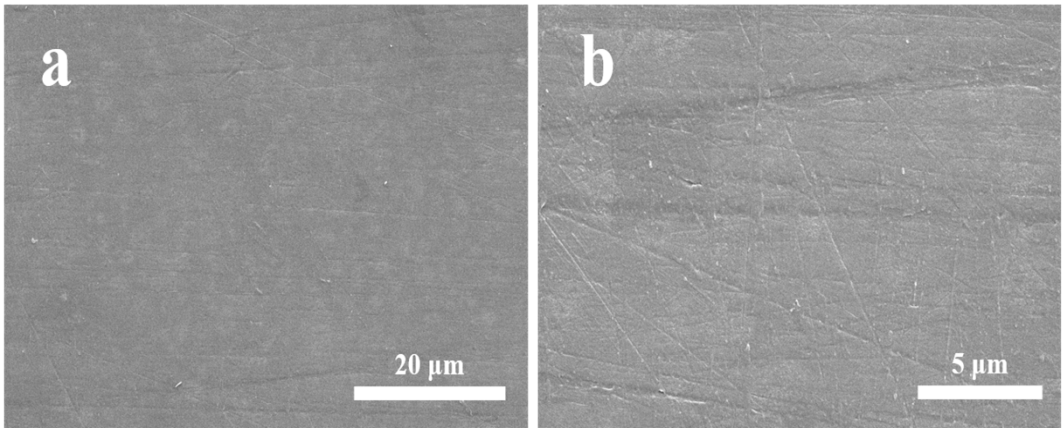

Fig. S8. (a-b) SEM images of the electrolysis products on the W cathode.

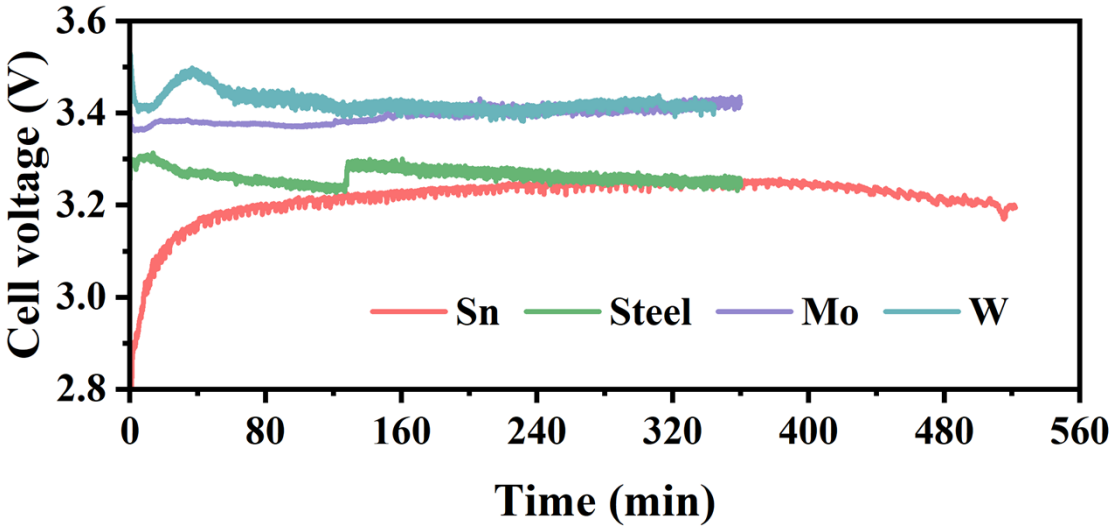

Fig. S9. Cell voltage of 0.4 A·cm^{-2} galvanostatic electrolysis using different cathodes under identical Mg^{2+} reduction.

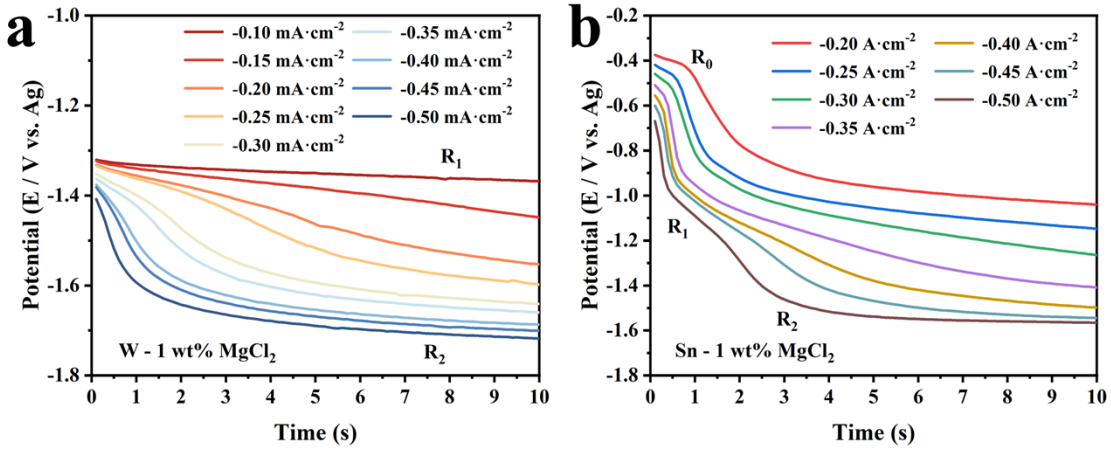

Fig. S10. Chronopotentiograms on (a) W and (b) Sn electrodes varied current density from -0.10 A·cm^{-2} to -0.50 A·cm^{-2}.

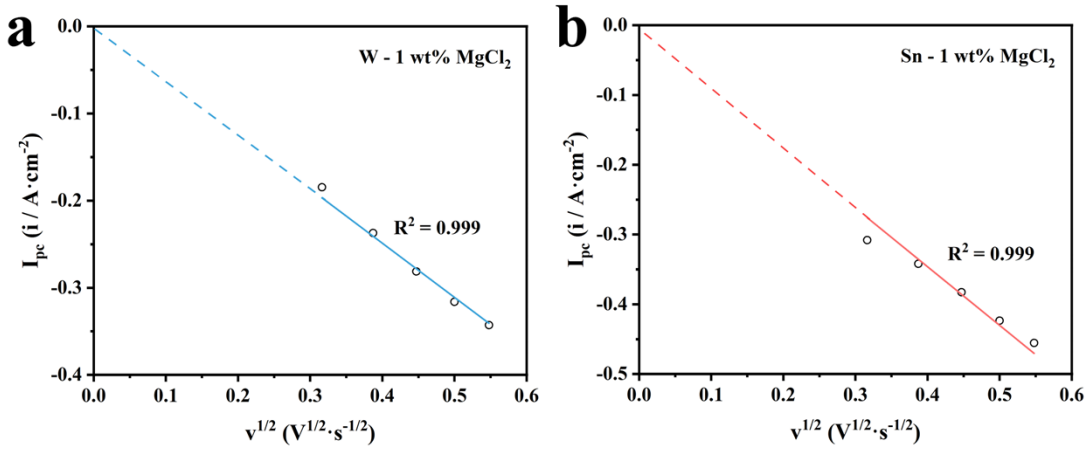

Fig. S11. Relationship between the square root of scan rate and peak current density on (a) W and (b) Sn electrodes.

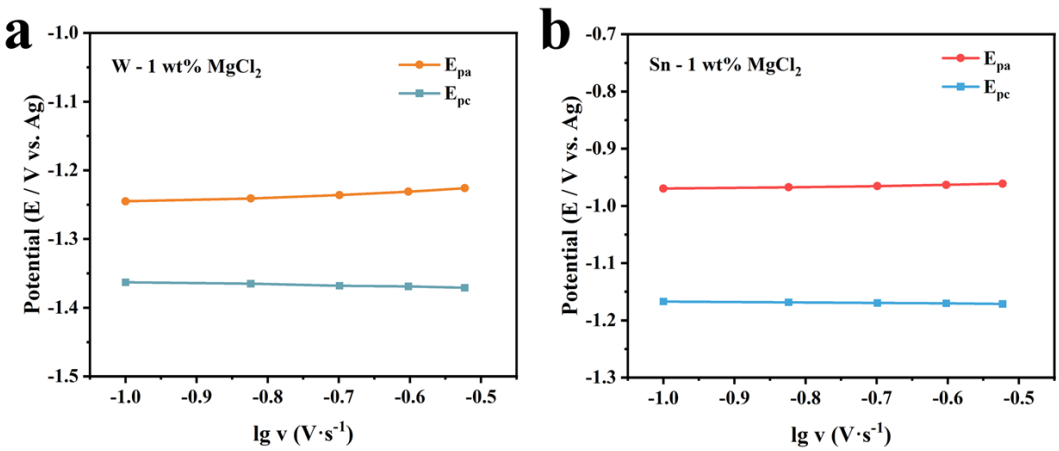

Fig. S12. Relationship between the logarithm of scan rate and peak potential on (a) W and (b) Sn electrodes.

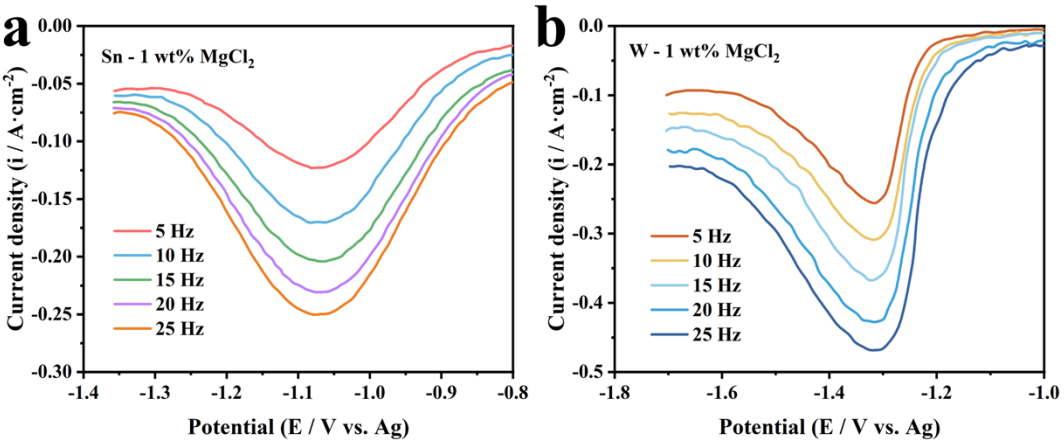

Fig. S13. Square wave voltammograms on (a) Sn and (b) W electrodes varied frequency from 5 Hz to 25 Hz.

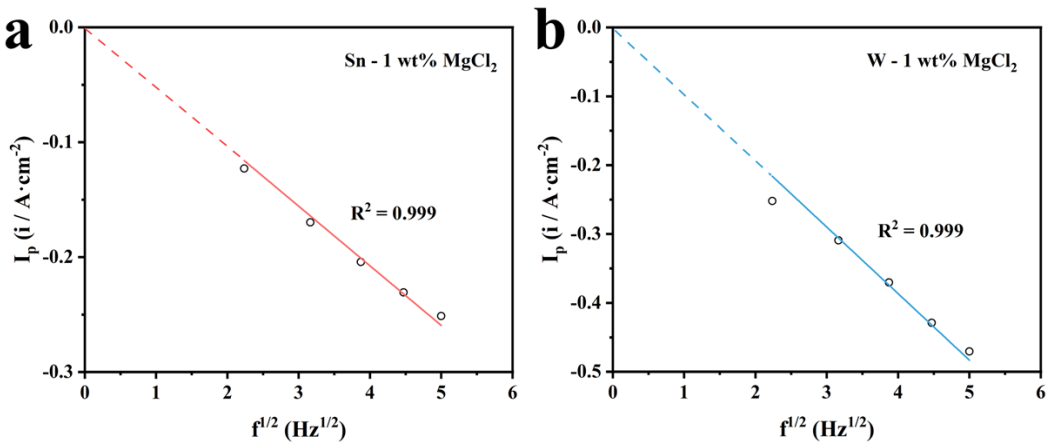

Fig. S14. Relationship between the square root of frequency and peak current density on (a) Sn and (b) W electrodes.

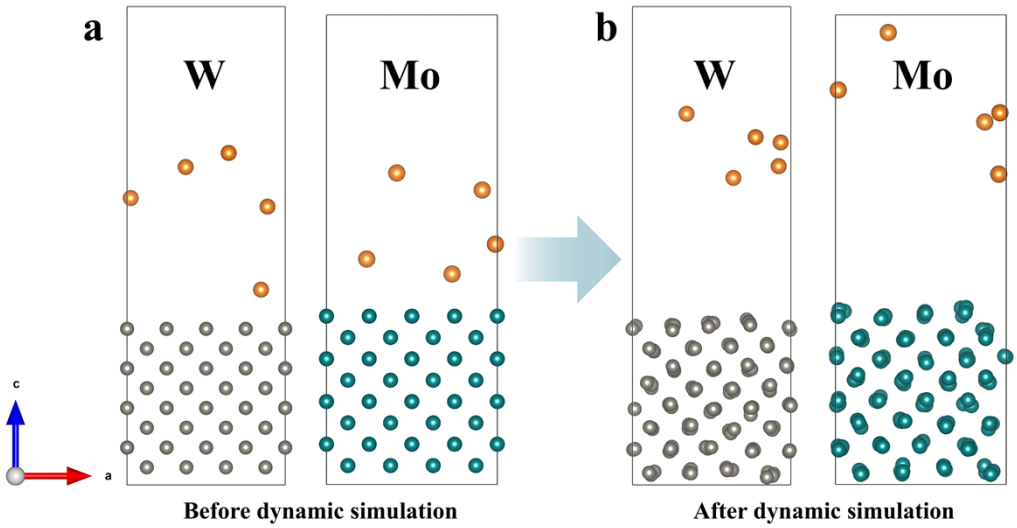

Fig. S15. The models of the W and Mo cathodes combined with Mg^{2+} (a) before and (b) after dynamic simulation.

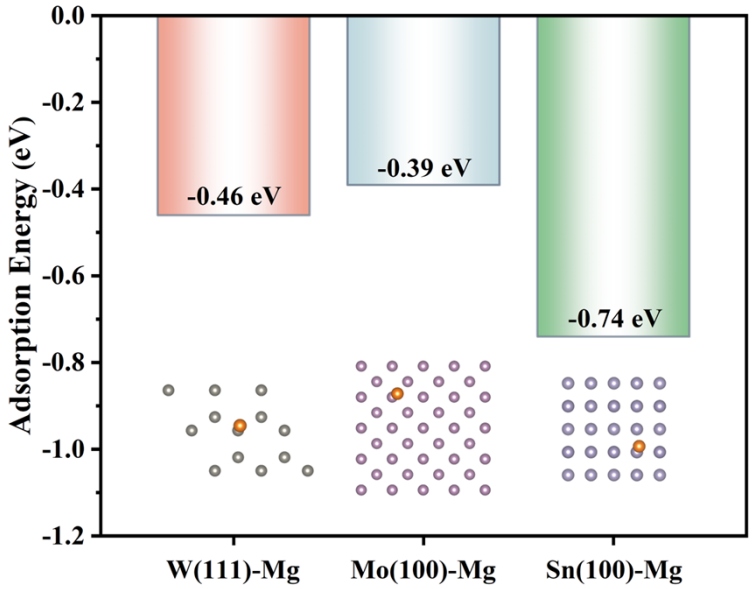

Fig. S16. The adsorption energy of W(111)-Mg, Mo(100)-Mg, and Sn(100)-Mg.

Supplementary tables

Table S1. The price of all molten salt.

Salt	Physical form	Purity	Price/£·kg^{-1}
LiCl	powder	99.5%	199.1
KF	powder	99.5%	21.8
$MgCl_2$	powder	99.5%	12.1
$CaCl_2$	powder	99.5%	11.6
KCl	powder	99.5%	7.7
NaCl	powder	99.5%	6.6

Table S2. Gibbs free energy calculation at 973 K.

Cathode	Reaction equation	ΔG/kJ·mol^{-1}	Potential/V
W	$2/3\ AlCl_3 = 2/3\ Al + Cl_2$	340.693	-1.7655
W	$MgCl_2 = Mg + Cl_2$	489.078	-2.5345
Sn	$Mg + 1/2\ Sn = 1/2\ Mg_2Sn$	-29.436	0.1526

Table S3. Comparison of current efficiency under different electrolysis parameters.

Current density	Anode working area	Electrolyte	Current efficiency
0.3 $A \cdot cm^{-2}$	3.9 cm^2	$MgCl_2$:NaCl:KCl=20:45:35	43%
0.3 $A \cdot cm^{-2}$	3.9 cm^2	$MgCl_2$:NaCl:KCl:$CaCl_2$:KF=18:40:30:10:2	65%
0.3 $A \cdot cm^{-2}$	3.9 cm^2	$MgCl_2$:NaCl:KCl:$CaCl_2$:KF=15:40:28:15:2	76%
0.4 $A \cdot cm^{-2}$	3.9 cm^2	$MgCl_2$:NaCl:KCl:$CaCl_2$:KF=15:40:28:15:2	82%
0.4 $A \cdot cm^{-2}$	7.1 cm^2	$MgCl_2$:NaCl:KCl:$CaCl_2$:KF=15:40:28:15:2	86%

Table S4. Change in product quality after electrolysis and current efficiency.

Time	Initial Sn	Product	Mg	Current efficiency
5.5 h	1 g	2.42 g	1.42 g	93%
8.8 h	1 g	3.14 g	2.14 g	89%
14.7 h	1 g	4.51 g	3.51 g	87%

Table S5. The properties of different metals.

	Melting point/K	Boiling point/K	Density
Mg	924	1380	1.74
Al	933	2740	2.70
Zn	692	1180	7.14
Sn	505	2533	7.31
Pb	600	2013	11.34
Ga	303	2676	5.90
Cd	594	1038	8.65
In	430	2333	7.30

Te	725	1663	6.25
Bi	544	1837	9.78
Sb	903	1908	6.68

Reference

1 L. Yang, Y. Yuan, Q. Li, J. Wu, T. Chen, J. Wang, X. Zuo, A. Tang, L. Zhang, N. Moelans and F. Pan, *Calphad*, 2023, **80**, 102524.

2 P. E. Blöchl, *Phys. Rev. B*, 1994, **50**, 17953–17979.

3 Y. Shi, W.-M. Huang, J. Li, Y. Zhou, Z.-Q. Li, Y.-C. Yin and X.-H. Xia, *Nat Commun*, 2020, **11**, 4558.